Polarized Raman Signals from Si Wafers: Dependence of In-Plane Incident Orientation of Probing Light

Woo Sik Yoo,[a,*,z] Hiroshi Harima,[b] and Masahiro Yoshimoto[b,*]

[a] *WaferMasters, Inc., San Jose, California 95112, USA*
[b] *Kyoto Institute of Technology, Matsugasaki, Sakyo, Kyoto 606-8585, Japan*

We report observations on polarization behavior of Raman signals from Si(100), Si(110) and Si(111) wafers depending on the orientation of in-plane probing light, in very high spectral resolution Raman measurements. Bare Si wafers were measured at the center of wafers, at 5° increments of wafer rotation, using a polychromator-based multiwavelength Raman system under 457.9, 488.0 and 514.5 nm excitation. Four-fold, two-fold and three-fold symmetrical oscillations of Raman intensity, shift and full-width-at-half-maximum (FWHM) were observed on Si(100), Si(110) and Si(111) wafers, respectively. In Si(100), intensity and FWHM showed their maximum at ⟨100⟩ directions, while Raman shift showed its maximum at ⟨110⟩ directions.
 [DOI: 10.1149/2.0061509jss]

Manuscript submitted June 22, 2015; revised manuscript received July 13, 2015. Published July 28, 2015.

This paper deals with understanding Raman Spectroscopy and its application to various crystal orientations ((100), (110) and (111)) of Si wafers for highly accurate measurements. Micro-Raman spectroscopy has been introduced as an optical characterization technique for various semiconductor materials.[1–6] Crystal structure, chemical composition and crystal orientation can be identified by a number of characteristics of the Raman peaks; their positions, intensity ratios, and their symmetry. The effect on Raman peaks of carrier concentration, impurity content, temperature and mechanical strain were studied extensively. As stress and strain engineering become an important part of advanced device design and manufacturing of high performance nanometer scale devices, unique non-destructive material characterization capabilities of micro-Raman spectroscopy in sub-micron applications, have been revisited in the last few years.[7–11] The lack of measurement accuracy, repeatability, spectral and spatial resolution, and frequent re-calibration to a reference crystal, has been preventing practical application of this technique in the semiconductor industry.

Although there are many publications on Raman characterization of Si, the exact Raman peak position (or wavenumber) is not well documented. This is mainly due to the poor resolution and measurement accuracy and repeatability of research oriented monochromator-based Raman systems with multi-functional designs using complex optical components. All optical components add distortion and attenuate light intensity.

Conventional monochromator-based Raman systems require frequent system calibration. The calibration is done both daily and between switching of excitation wavelength using a reference crystal and/or plasma lines of a laser. However, Raman papers report different values of the stress-free Si peak, in the range of 520 ∼ 522 cm^{-1}. Some papers even report different values throughout the paper, noting this calibration problem.[1] Advanced stress and strain engineered devices require at least 50 MPa of stress sensitivity. This requires wavenumber resolution and (short term and long term) measurement repeatability of approximately 0.1 cm^{-1} before curve fitting of measured spectra, for meaningful Raman characterization. Most Raman studies utilize low resolution measurements with as-measured resolution in the range of 0.5 ∼ 3.0 cm^{-1}/pixel and are curve fitted to detect a peak shift of almost 0.1 cm^{-1}, which exceeds their resolution capability. Since one wavenumber (1 cm^{-1}) is equivalent to 434 MPa of stress[2], the uncertainty of 2 cm^{-1} in the stress-free Si peak can lead to misinterpretation of 868 MPa of stress, and possibly the direction of the stress (compressive or tensile). The measurement uncertainty is 20 times larger than the wavenumber resolution required for proper characterization of advanced stress and strain engineered devices. Curve fitting using data that is below the resolution capability, is highly questionable.

The 0.1 cm^{-1} Raman shift of the Si peak under 457.9 and 488.0 nm excitation is equal to 2.115 and 2.404 pm in wavelength, respectively. It becomes 2.673 pm at the Si Raman peak under 514.5 nm excitation. The unique, no-moving-part design of the multiwavelength Raman spectroscopy system minimizes the uncertainties in absolute wavenumber of the Raman signal by eliminating the common mechanical problems,[12–17] such as calibration errors, optical misalignment from vibration, and backlash of moving parts, seen in conventional Raman systems. This is to get the measurement resolution, stability and repeatability required to make useful determination of these physical characteristics of a Si wafer.

The main focus of the new design was to achieve the highest possible measurement resolution, accuracy, repeatability, excitation wavelength flexibility and productivity. The unique polychromator design, with a very long focal length (2.0 m) focusing mirror with wide spectrum coverage and three charge coupled device (CCD) cameras for measuring Raman signals from three individual excitation wavelengths, made sequential Raman measurement possible under different excitation wavelengths without re-calibration. The elimination of moving parts in the polychromator has significantly enhanced spectral resolution, accuracy and repeatability of measurement. Three major spectral lines (457.9, 488.0 and 514.5 nm), from a multi-wavelength Ar^+ ion laser, are used as the excitation source, which allow crystal quality, stress and strain to be characterized at different depths.[12–17] The configuration of the polychromator-based multiwavelength Raman system is illustrated in Fig. 1.

Raman signals from a bare Si (100) reference wafer, under all three excitation wavelengths, are centered at 520.3 cm^{-1} and are highly symmetrical.[12–14] The symmetry of the Raman signal suggests that the system has extremely low image distortion. The wavenumber resolution at the excitation wavelengths of 457.9, 488.0 and 514.5 nm are 0.105, 0.085, and 0.071 cm^{-1}/pixel, respectively, before curve fitting. Variations in Raman shift and full-width-at-half-maximum (FWHM) of Raman signals, from the same reference Si (100) sample, was monitored for three months at all three excitation wavelengths, to verify the designed performance of the system.[17] The measurement variation or uncertainty during the three month monitoring period was less than 0.05 cm^{-1}. Both highly reliable and high resolution Raman studies on semiconductor materials become possible.

Longitudinal optical (LO) phonons are observed from Si (100) in a back scattering geometry. From a Si (110) (cleaved wafer), slight differences in Raman spectra are expected due to differences in polarization. In the absence of stress, three optical Raman modes of Si are believed to be degenerate and are expected to have the same wavenumber.[1] Scientists have empirical knowledge of the strong angular dependence of Raman intensity for Si (100) in back scattering

*Electrochemical Society Active Member.
[z]E-mail: woosik.yoo@wafermasters.com

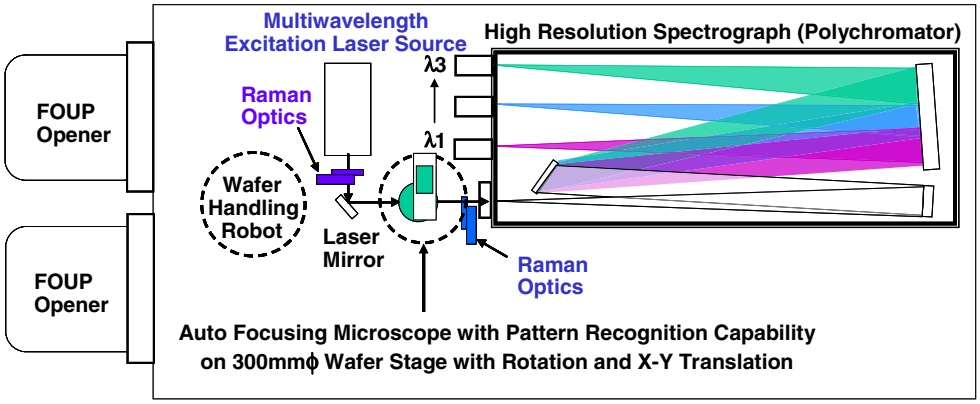

Figure 1. Schematic illustration of the polychromator-based, multiwavelength Raman spectroscopy system.

geometry measurements.[1,2,18] They often position the samples in a way that Raman intensity is maximized, to shorten data acquisition time and to improve signal-to-noise ratio. It is also assumed that in-plane sample rotation does not affect the Raman shift and FWHM values measured. Due to insufficient wavenumber resolution characteristic of typical Raman systems, with poor measurement accuracy and repeatability, it was almost impossible to make accurate absolute measurements. All measurements were compared to their reference samples.

In-plane angular dependence of Raman intensity, shift and FWHM of 300 mm diameter Si (100) wafers have been investigated under 457.9, 488.0 and 514.5 nm excitation. A wafer was centered on the measurement stage and Raman signals from the center of Si (100) wafer under 457.9, 488.0 and 514.5 nm excitation were sequentially measured, without calibration between wavelength switching. To make sure all the measurements during rotation were done from the same exact point on the wafer, the wafer was centered on a rotation stage and the center of the center rotation stage was aligned to an objective lens of the Raman microscope (Fig. 2). The measurements were repeated by rotating the wafer from 0 to 360° in 5° counter clockwise steps. The notch direction of ⟨110⟩ is referred as 0°. Similar experiments were done using smaller diameter (50 mm) Si wafers with three different crystal orientations ((100), (110) and Si (111)) to study the dependence of in-plane incident orientation of probing light, with respect to atomic arrangements, on the surface of Si wafers with different orientations. For simplicity, experimental results from Si (100) wafers are mainly discussed in this paper.

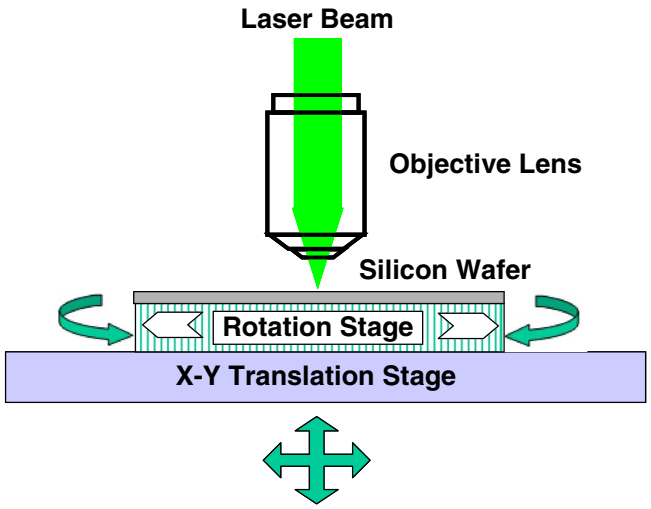

Figure 2. Illustration of experimental configuration for angular dependence Raman measurement study.

Figures 3a and 3b show Raman shift, FWHM and intensity as a function of wafer rotation angle under three different excitation wavelengths. All three parameters showed strong in-plane angular dependence for Si (100), even though the peaks and valleys of individual parameters appear at different angles from each other. The peaks and valleys of Raman shifts and FWHM appear in opposite phases. The Raman shift minima and maxima occur in the ⟨100⟩ direction and ⟨110⟩ direction, respectively. The FWHM maxima and minima both occur in the ⟨110⟩ direction, but are 45° out of phase from each other. The intensity maxima and minima follow the trend of FWHM angular dependency. The maximum intensity can be approximately 2 times the minimum intensity, depending on the excitation wavelength. The Raman shift varied from 520.30 cm^{-1} in the ⟨100⟩ direction to 520.45 cm^{-1} in the ⟨110⟩ direction. The FWHM variation range is 0.20 cm^{-1}.

Figure 4 shows the polar plots of Raman shift, FWHM and intensity data used in Fig. 3. In-plane angular dependence under all three excitation wavelengths is clearly demonstrated. The magnitude of variations of the three parameters showed slight dependence on excitation wavelength. This can be interpreted as the difference in probing depth (probing volume) and intrinsic FWHM performance of the Raman system, at each excitation wavelength. The intrinsic FWHM of the Raman system is determined by the probing laser beam quality (coherency or line width of laser wavelength), the dispersion of the diffraction grating, pin hole size (or entrance slit width) and quality (degree of distortion) of the optical components used in the light path of the spectrometer.

To understand the symmetry (atomic arrangement and chemical bonds) of the Si (100), unit cell of diamond structure Si crystal, a top view atomic arrangement with chemical bond directions is illustrated in Fig. 5. For easy recognition, Si atoms on different layers in the unit cell were illustrated by spheres with different colors. The Si (100) surface shows four-fold symmetry in atomic arrangement and chemical bonds. All chemical bonds are aligned in the four equivalent ⟨110⟩ directions. The direction of maximum Raman shift is in good agreement, in the ⟨110⟩ equivalent directions, with chemical bonds (discussed later). The FWHM and intensity maxima appear in the ⟨100⟩ directions with no chemical bonds. Back scattering from a Si (100) surface by LO phonons, in-plane polarized along the incident direction, is visible regardless of wafer rotation.

The orientation dependence of Raman intensity (Fig. 3b and Fig. 4c) can be easily explained by the selection rules of Raman peak from a Si crystal with ideal diamond structure. However, the orientation dependence of the Raman shift and FWHM (Fig. 3a, and Figs. 4b and 4c) cannot be explained, even if we assume that there is simple residual stress in the Si (100) crystal. The most likely cause of this orientation dependence is the interaction from the in-plane incident orientation dependence of a (polarized) Raman signal by Si

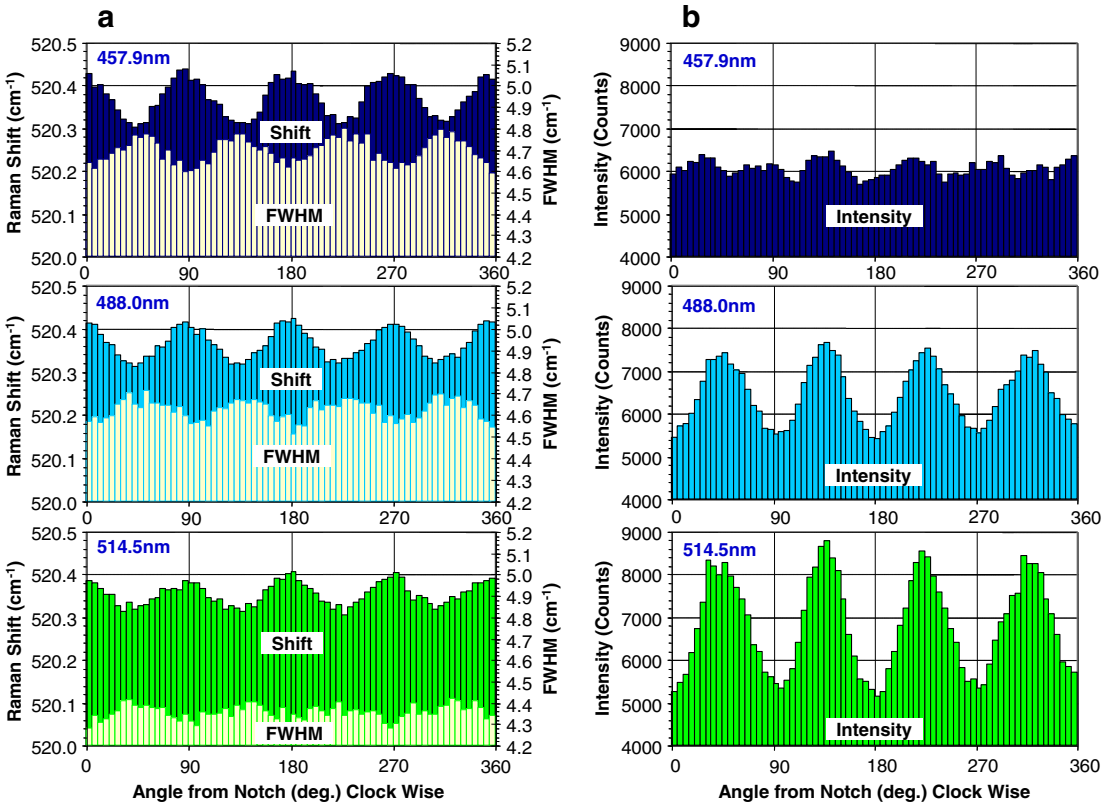

Figure 3. Wafer orientation dependence of (a) Raman shift and FWHM, and (b) intensity of Si peak from a Si (100) wafer under various excitation wavelengths (counter clockwise rotation in 5 degree increments).

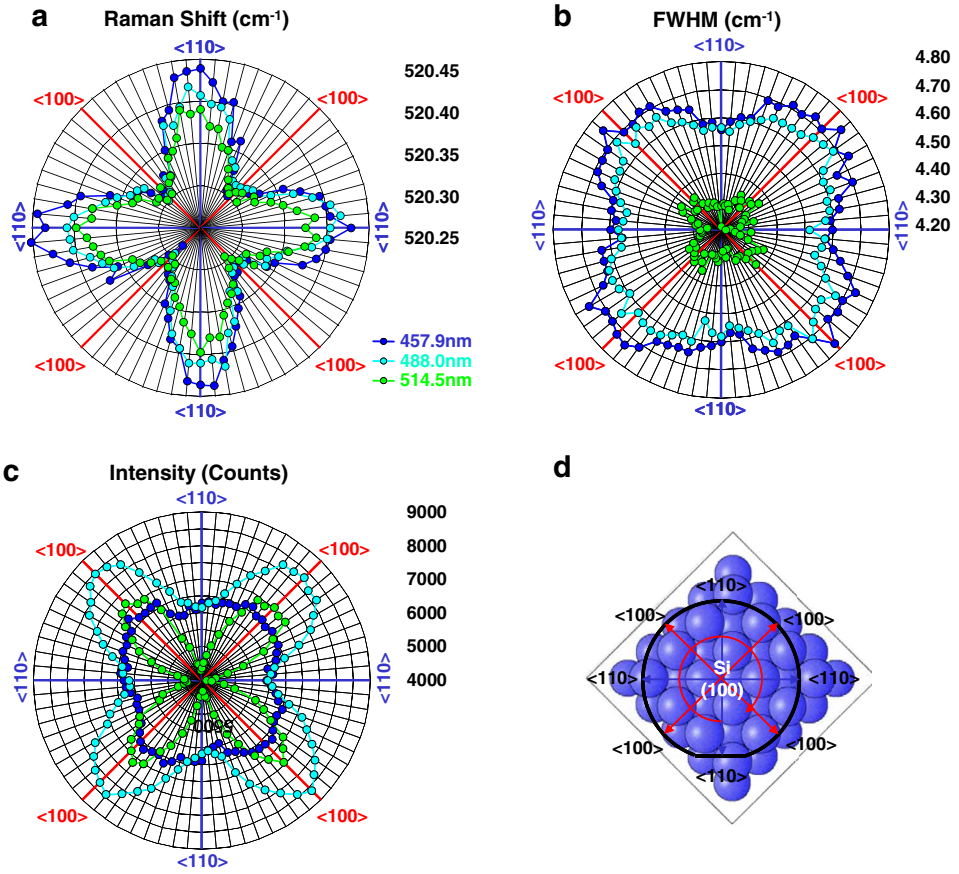

Figure 4. Wafer orientation dependence of (a) Raman shift, (b) FWHM, (c) intensity of the Si peak from a Si (100) wafer under various excitation wavelengths (counter clockwise rotation in 5 degree increments) and (d) equivalent crystallographical orientations on the Si (100) wafer.

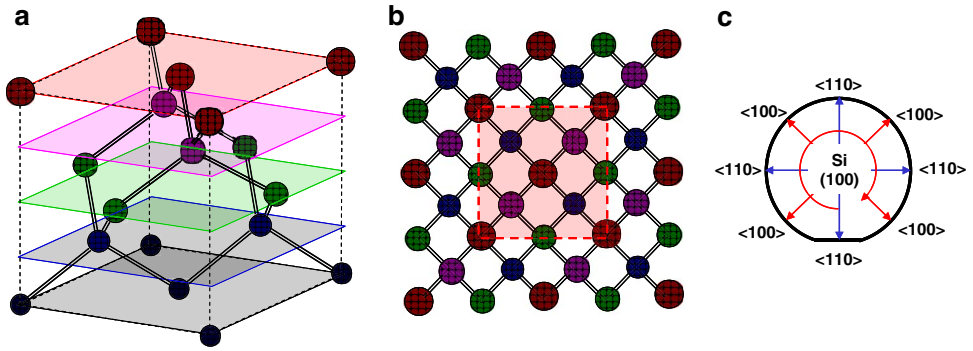

Figure 5. (a) Unit cell of the Si crystal structure, (b) top view of atomic arrangement of the Si (100) surface with equivalent crystallographic orientations and (c) equivalent crystallographical orientations on a Si (100) wafer.

(100) crystal and polarization characteristics of the spectrograph determined by the configuration (slit width, diffraction grating, CCD (charge coupled device) photo detector). Polarization of light by (reflection and scattering from) a crystal surface, narrow slits, and diffraction gratings are well known.[19–22] Even if the light is completely blocked by crossed polarizers, the insertion of a third polarizer between the crossed polarizers can allow some light to pass.[23,24] Thus, the wafer rotation modulated the polarization of scattered Raman signal and interacted with the inherent polarization characteristics of the spectrograph. Considering the symmetry of atomic arrangements and chemical bonds, the in-plane angular dependence of Raman intensity, shift and FWHM is evident.[25] Many physical properties (such as Young's modulus, Poisson's ratio, piezoresistance etc.) of the Si crystal depend on crystal orientation.[26,27] Anisotropic carrier transport properties of Si are actively utilized in advanced nanometer scale, high performance electronic devices today.[28,29] It may be a very unlikely event, but we cannot completely rule out the possibility of the presence of complex residual stress in semiconductor manufacturing grade Si (100) as one of the possible origins of the orientation dependence.

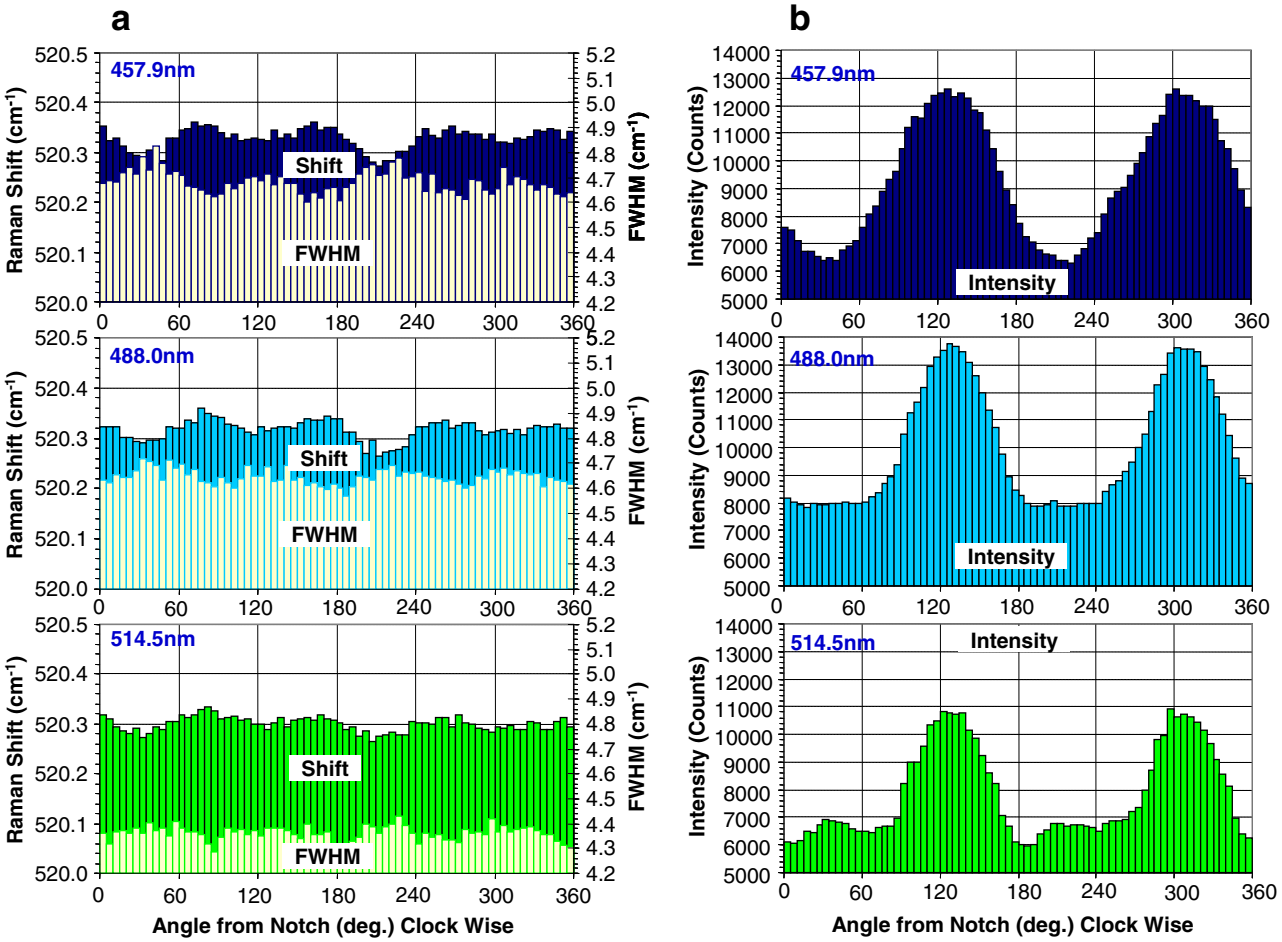

Figure 6. Wafer orientation dependence of (a) Raman shift and FWHM, and (b) intensity of Si peak from a Si (110) wafer under various excitation wavelengths (counter clockwise rotation in 5 degree increments).

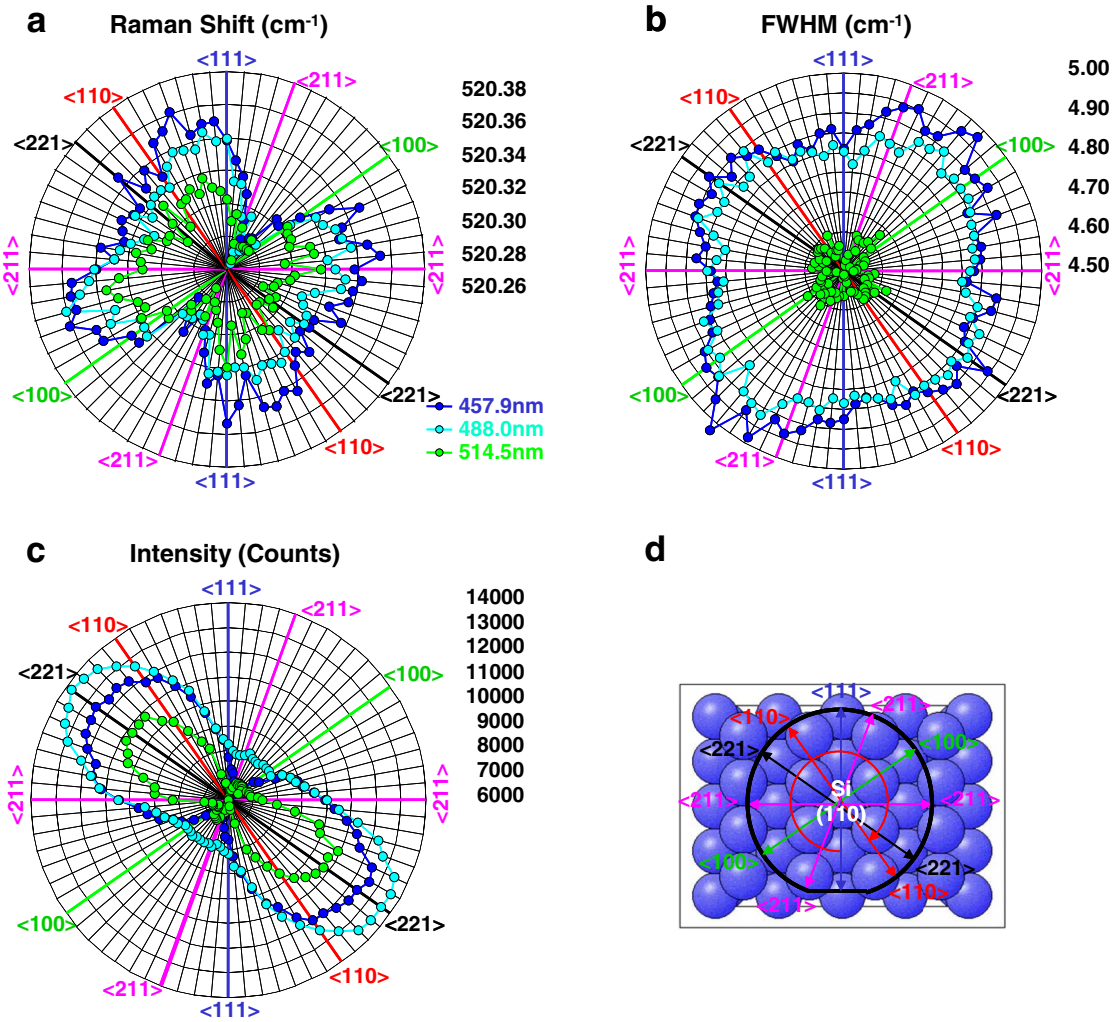

Figure 7. Wafer orientation dependence of (a) Raman shift, (b) FWHM, (c) intensity of the Si peak from a Si (110) wafer under various excitation wavelengths (counter clockwise rotation in 5 degree increments) and (d) equivalent crystallographical orientations on the Si (110) wafer.

The excitation wavelength dependence of all three Raman parameters is also somewhat unclear. However, the trends are the same and phenomena are very repeatable. It is likely that the dependence of polarization amplitude on the Si surface (crystal orientation and chemical bond orientation with respect to electromagnetic (EM) field of probing light) is an important factor. Since the only moving component was the Si wafer, the in-plane incident orientation of probing light was the only variable in this study. To verify the origin of in-plane incident angle dependence of the three Raman parameters, we have measured Raman signals from Si (110) and Si (111) wafers. We have found two-fold symmetry dependence from Si (110) wafers and three-fold symmetry dependence from Si (111) wafers. The angular dependence of Raman signals shows good agreement with atomic arrangement and chemical bond directions of the top surface of the Si.

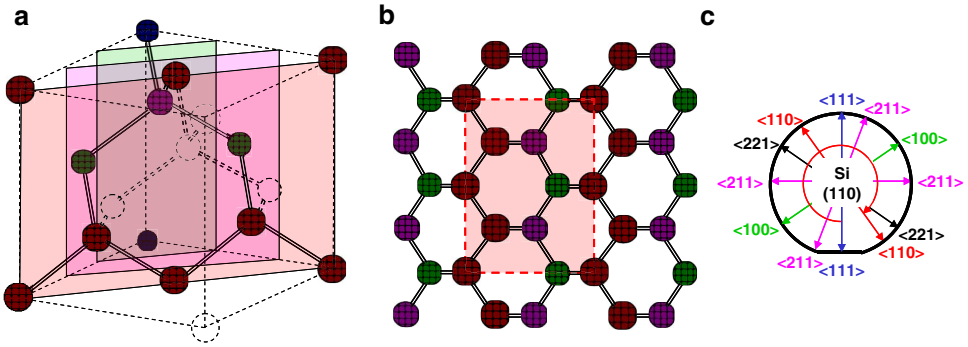

Figure 8. (a) Unit cell of the Si crystal structure, (b) top view of atomic arrangement of the Si (110) surface with equivalent crystallographic orientations and (c) equivalent crystallographical orientations on a Si (110) wafer.

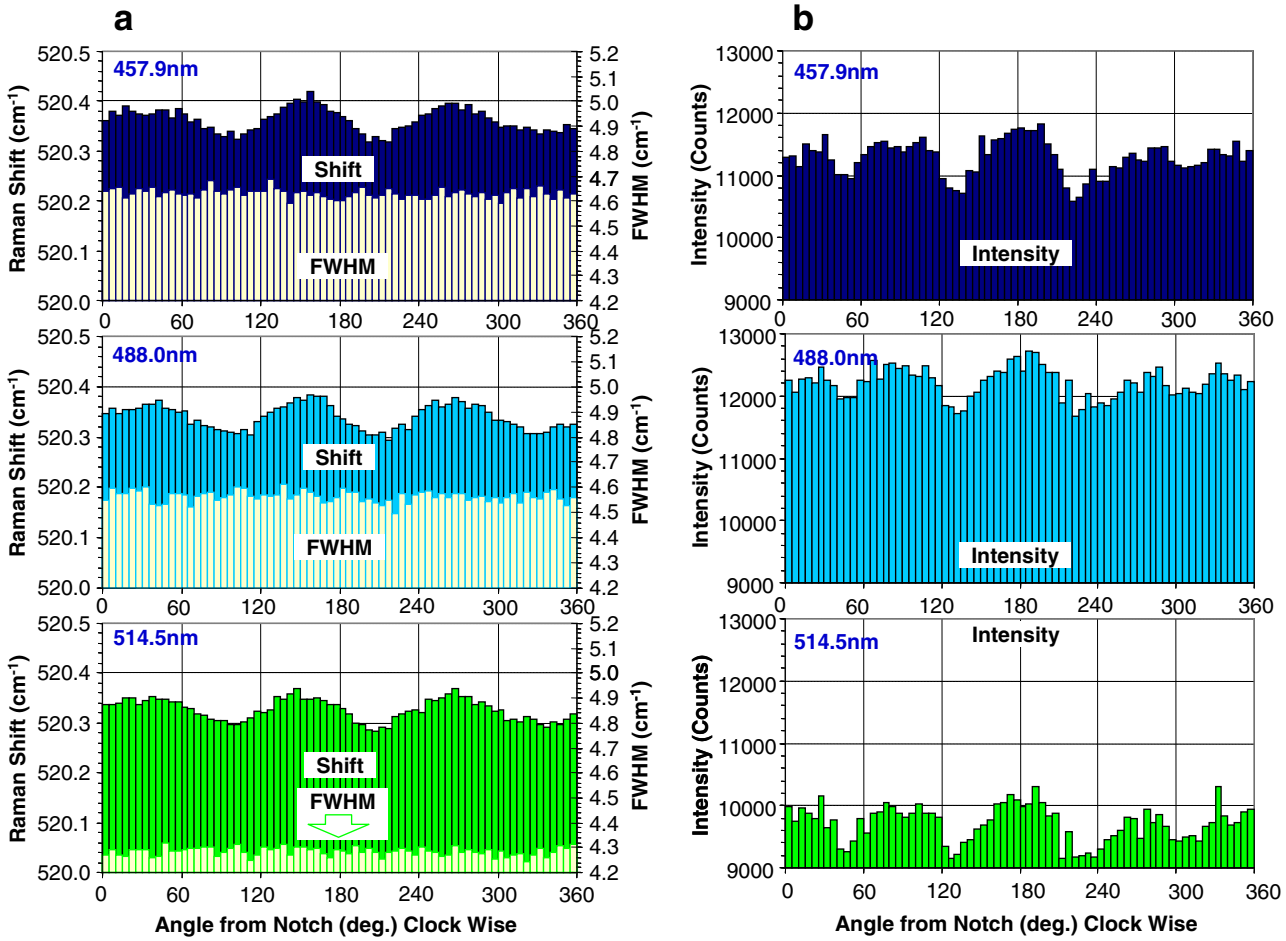

Figure 9. Wafer orientation dependence of (a) Raman shift and FWHM, and (b) intensity of the Si peak from a Si (111) wafer under various excitation wavelengths (counter clockwise rotation in 5 degree increments).

For Si (110) wafers, Figs. 6a and 6b show Raman shift, FWHM and intensity as a function of wafer rotation angle under three different excitation wavelengths. Figure 7 shows the polar plots of Raman shift, FWHM and intensity data used in Fig. 6. A unit cell of the Si crystal structure and top view of atomic arrangement of the Si (110) surface, with equivalent crystallographic orientations, are illustrated in Fig. 8.

For Si (111) wafers, Raman shift, FWHM and intensity, as a function of wafer rotation angle under three different excitation wavelengths, are shown in Figs. 9a and 9b. The polar plots of Raman shift, FWHM and intensity are shown in Fig. 10. Figure 11 illustrates the unit cell of the Si crystal structure and top view of atomic arrangement of Si (111) surface with equivalent crystallographic orientations.

We have measured Raman signals from Si (100) wafers with various films (such as SiO_2, SiN, SiGe, NiSi, CoSi and NiSi) and found identical in-plane angular dependence. In epitaxial $Si_{1-x}Ge_x$/Si(100) wafers, we have measured the in-plane incident angle dependence of the three Raman parameters of Si-Si peak at ~510 cm^{-1} for a $Si_{0.7}Ge_{0.3}$ epitaxial layer and Si-Si peak for a Si wafer at ~520 cm^{-1} to verify the epitaxial relationship. We verified the epitaxial relationship from the alignment of four-fold symmetry of the two Si-Si peaks at ~510 cm^{-1} and ~520 cm^{-1}. No measurable disorientation between the $Si_{0.7}Ge_{0.3}$ epitaxial layer and Si wafer was detected from the angular dependence of three Raman parameters of Si-Si peak from the $Si_{0.7}Ge_{0.3}$ epitaxial layer at ~510 cm^{-1} and the Si-Si peak from the Si wafer at ~520 cm^{-1}.

One wavenumber (1 cm^{-1}) shift in Raman peak is equivalent to a lattice vibration energy of 120 μeV. The variation of Raman shift due to the in-plane angular dependence was ~0.15 cm^{-1}, which is approximately 18 μeV variation in energy. Thermal energy at room temperature (300 K) is approximately 20 meV (kT/e). Detection of a 0.15 cm^{-1} (or 18 μeV) difference in room temperature measurements is worth noting. In this study we have recognized and demonstrated the sensitivity of Raman spectroscopy to the electronic state and orientation of the Si crystal. This technique can also be used as an alternative to the time consuming X-ray reciprocal space map (RSM) measurement in the field of high resolution thin heteroepitaxial film characterization technique.[30,31]

In summary, we have observed in-plane angular dependence of Raman intensity, shift and FWHM from Si wafers with three different crystal orientations of (100), (110) and (111). Four-, two- and three-fold symmetries of three Raman parameters were measured corresponding to the chemical bond arrangement (atomic arrangement) of the surface of Si (100), (110) and (111), respectively. The Raman shift and FWHM variations in Si (100) wafers were 0.15 and 0.20 cm^{-1}, respectively, depending on wafer rotation relative to the polarization of the excitation laser beam. For precise measurement and proper interpretation of Raman signals with accuracy of 0.1 cm^{-1}, required in characterization of advanced devices, a multiwavelength, high resolution Raman system with high measurement repeatability must be used, and the in-plane angular dependence of Raman signal must be considered. High resolution Raman measurement capability of the newly developed Raman system opens up a new field of exciting research and deepens our understanding of the electronic structure of crystals.

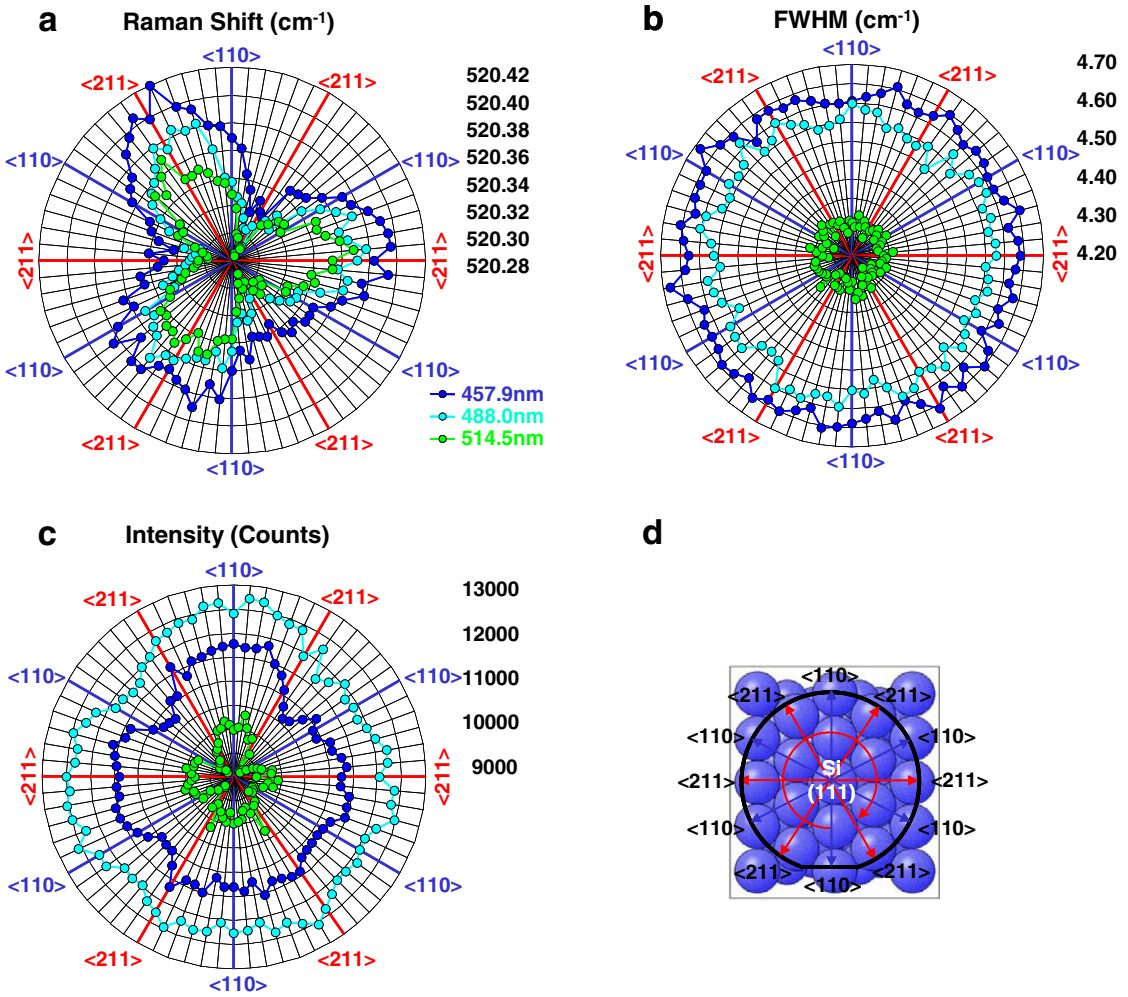

Figure 10. Wafer orientation dependence of (a) Raman shift, (b) FWHM, (c) intensity of Si peak from a Si (111) wafer under various excitation wavelengths (counter clockwise rotation in 5 degree increments) and (d) equivalent crystallographical orientations on a Si (111) wafer.

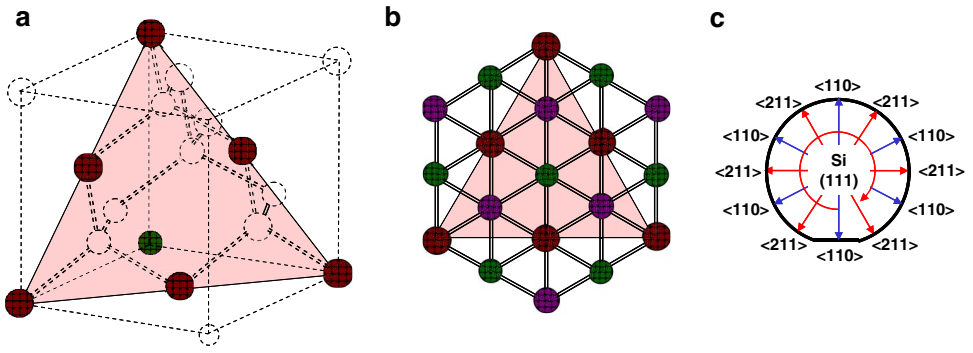

Figure 11. (a) Unit cell of the Si crystal structure, (b) top view of atomic arrangement of the Si (111) surface with equivalent crystallographic orientations and (c) equivalent crystallographical orientations on a Si (111) wafer.

Acknowledgments

The authors thank Takeshi Ueda, Kitaek Kang and James Schram of WaferMasters, Inc. for their experimental assistance and useful discussions.

References

1. I. DeWolf, *Semicond. Sci. Technol.*, **11**, 139 (1996).
2. I. De Wolf, *Spectroscopy Europe*, **15/2**, 6 (2003).
3. H. Harima, S. Nakashima, J. M. Carulli, C. P. Beetz, and W. S. Yoo, *Jpn. J. Appl. Phys.*, **36**, 5525 (1997).
4. H. Harima, *J. Phys. Condens. Matter*, **14**, R967 (2002).
5. H. Harima, *Proc. 14th IEEE Int. Conf. Advanced Thermal Processing of Semiconductors*, Kyoto, 2006, p.117.
6. D. Olego and M. Cardona, *Phys. Rev. B*, **23**, 6592 (1981).
7. M. Belyansky, A. Domenicucci, N. Klymko, J. Li, and A. Madan, *Solid State Technol.*, **52**(2), 26 (2009).
8. A. Ogura, K. Yamasaki, D. Kosemura, S. Tanaka, I. Chiba, and R. Shimidzu, *Jpn. J. Appl. Phys.*, **45**, 3007 (2006).
9. J. P. Liu, K. Li, S. M. Pandey, F. L. Benistant, A. See, M. S. Zhou, L. C. Hsia, R. Schampers, and D. O. Klenov, *Appl. Phys. Lett.*, **93**, 221912 (2008).

10. R. Z. Lei, W. Tsai, I. Aberg, T. B. O'Reilly, J. L. Hoyt, D. A. Antoniadis, H. I. Smith, A. J. Paul, M. L. Green, J. Li, and R. Hull, *Appl. Phys. Lett.*, **87**, 251926 (2005).
11. O. Moutanabbir, M. Reiche, A. Hähnel, M. Oehme, and E. Kasper, *Appl. Phys. Lett.*, **97**, 053105 (2010).
12. W. S. Yoo, T. Ueda, and K. Kang, *Ext. Abstr. Int. Conf. Solid State Devices and Materials, Tsukuba*, 2008, p. 376.
13. W. S. Yoo, T. Ueda, T. Ishigaki, and K. Kang, *Ext. Abstr. 9th Int. Workshop Junction Technology*, Kyoto, 2009, p. 79.
14. W. S. Yoo, T. Ueda, T. Ishigaki, and K. Kang, *Proc. 17th IEEE Int. Conf. Advanced Thermal Processing of Semiconductors*, Albany, 2009, p. 175.
15. W. S. Yoo, K. Kang, T. Ueda, and T. Ishigaki, *Appl. Phys. Express*, **2**, 116502 (2009).
16. A. D. Trigg, L. H. Yu, C. K. Cheng, R. Kumar, D. L. Kwong, T. Ueda, T. Ishigaki, K. Kang, and W. S. Yoo, *Appl. Phys. Express*, **3**, 086601 (2010).
17. Y. F. Tzeng, S. Ku, S. Chang, C. M. Yang, C. S. Chern, J. Lin, N. Hasuike, H. Harima, T. Ueda, T. Ishigaki, K. Kang, and W. S. Yoo, *Appl. Phys. Express*, **3**, 106601 (2010).
18. D. Tuschel, *Spectroscopy*, **27**(3), 22 (2012).
19. C. Palmer, *Diffraction Grating Handbook*, 6th Eds., (Newport Corp., New York, 2005) Chap. 8.
20. R. V. Jones and J. C. S. Richards, *Proceedings A*, **225**(1160), 122 (1954).
21. D. Halliday and R. Resnick, *Physics Part 2 Extended Version*, (John Wiely & Sons, New York, 1986) Chap. 48.
22. *Handbook of Chemistry and Physics 75th Edition*, D. R. Lide Editor-in-Chief. (CRC Press, Boca Raton, Florida, 1994) Section 10.
23. R. C. Jones, *J. of the Optical Society of America*, **46**(7), 528 (1956).
24. J. M. Liu, *Photonic Devices*, (Cambridge University Press, Cambridge, 2005) Part I.
25. V. Darakchieva, T. Paskova, M. Schubert, H. Arwin, P. P. Paskov, B. Monemar, D. Hommel, M. Heuken, J. Off, F. Scholz, B. A. Haskell, P. T. Fini, J. S. Spek, and S. Nakamura, *Phys. Rev. B*, **75**, 195217 (2007).
26. J. Kim, D. Cho, and R. S. Muller, *Transducers '01. Eurosensors XV*, **1**, 662 (2001).
27. D. Colman, R. T. Bate, and J. P. Mize, *J. Appl. Phys.*, **39**, 1923 (1968).
28. N. Mohta and S. E. Thompson, *IEEE Circuits & Devices Magazine*, Sept./Oct. (2005) P. 23.
29. S. E. Thompson, S. Guangyu, C. Youn Sung, and T. Nishida, *IEEE Trans. Electron Devices*, **53**, 1010 (2006).
30. S. Kobayashi and K. Inaba, *The Rigaku Journal*, **28**(1), 8 (2012).
31. B. B. He, *Two-dimensional X-Ray Diffraction*, (John Wiely & Sons, Hoboken, New Jersey, 2009) Chap. 1.